Size-fraction specific isotopic variations as a framework for interpreting early Paleogene bulk sediment carbon isotope records

Joyeeta Bhattacharya[1]*, Laurence Y. Yeung[1], Lin Cong[2], Gerald R. Dickens[1,3], and Tao Sun[1]

[1]Department of Earth, Environmental and Planetary Sciences, Rice University, Houston, TX, USA

[2]Northeast Petroleum University, Daqing, China

[3]Trinity College, Dublin, Ireland

*Corresponding author email id: jb79@rice.edu

Key points

1. Co-evolution of different components within pelagic carbonate systems drive spatial variations of bulk carbonate stable isotope records.
2. Increase in coarse fraction abundance across PETM at Shatsky Rise alters the conventional implications of using it as a dissolution proxy.
3. Size-fraction-specific isotopic variations can also significantly control the magnitude of carbon isotope excursions.

Abstract

Carbon isotope ($\delta^{13}C$) records from marine sediments have been extensively used in Cenozoic chemostratigraphy. The early Paleogene interval in particular has received exceptional attention because negative carbon isotope excursions (CIEs) documented in the sedimentary record, e.g. at the Paleocene Eocene Thermal Maximum (PETM), ca ~56 Ma, are believed to reflect significant global carbon cycle perturbations during the warmest interval of the Cenozoic era. However, while bulk-carbonate $\delta^{13}C$ values exhibit robust correlations across widely separated marine sedimentary sections, their absolute values and magnitude of CIEs vary spatially. Moreover, bulk-carbonates in open-marine environments are an ensemble of different components, each with a distinct isotopic composition. Consequently, a complete interpretation of the bulk $\delta^{13}C$ record requires an understanding of co-evolution of these components. In this study, we dissect sediments, from early Paleogene interval, at ODP Site 1209, Shatsky Rise, Pacific Ocean to investigate how an evolving bulk-carbonate ensemble influences the overall carbon isotope record. A set of 45 samples were examined for $\delta^{13}C$ and $\delta^{18}O$ compositions, as bulk and individual size fractions. We find a significant increase in coarse-fraction abundance across PETM, driven by a changing community structure of calcifiers, modulating the size of CIE at Site 1209 and thus making it distinct from those recorded at other open-marine sites. These results highlight the importance of biogeography in marine stable-isotope record, especially when isotopic excursions are driven by climate- and/or carbon-cycle changes. In addition, community composition changes will alter the interpretation of weight percent coarse fraction as conventional proxy for carbonate dissolution.

Key words

Carbon Isotope Excursions, Chemostratigraphy, PETM, Hyperthermals, Coarse fraction, Bulk Carbonates

1. Introduction

Carbon isotope records of the Cretaceous and Cenozoic are commonly obtained using analysis of open marine carbonate sediments (e.g. Shackleton 1986; Shackleton et al., 1987; Reghellin et al., 2015). A substantial amount of work using bulk carbonate $\delta^{13}C$ records focuses on the early Paleogene period (e.g. Quillévéré et al., 2008; Slotnick et al., 2015; Luciani et al., 2016; Westerhold et al. 2017), which had a hothouse climate and was the warmest interval of the Cenozoic (e.g. Zachos et al., 2001; 2008). Temporal variations in bulk carbonate $\delta^{13}C$ values from widely separated ocean sites are remarkably consistent during the early Paleogene, thus forming a robust tool of stratigraphic correlation between marine sedimentary sections (e.g. Slotnick et al, 2012; Agnini et al, 2015; Westerhold et al, 2018; Barnet et al, 2019; D'Onofrio et al., 2020). However, differences in their absolute values suggest that subtle differences in palaeoceanographic context are also recorded alongside large-scale changes in carbon cycling and climate.

One manifestation of the palaeoceanographic context may be the community structure of calcifiers, because bulk carbonates in open marine environments are generally an ensemble of various biogenic components (**Figure 1**). At a simple level of classification, calcifiers can be readily grouped as either pelagic or benthic. Calcareous nannoplanktons predominate the group of pelagic calcifiers by abundance, followed by planktic foraminifers (e.g. Bralower et al., 2002; Reghellin et al., 2020). Benthic foraminifers, in contrast, generally constitute a small proportion of bulk carbonates (Milliman, 1993; Sarmineto and Gruber, 2006; Cramer et al, 2009). Each of these calcifying groups, further comprised of a multitude of genera, dwell at different depth in the water column and express different isotopic fractionation during carbonate precipitation; therefore, their carbonate shells have distinct carbon and oxygen isotope signatures (**Figure 1**). Furthermore, these calcifiers exhibit varying degrees of susceptibility to carbonate dissolution (e.g. Petrizzo et al., 2008;

64 Nguyen et al., 2009). All such factors contribute towards resultant heterogeneity in bulk carbonates
65 across time and space.

66 In the early Paleogene sediment sections of Shatsky Rise (in the tropical north-central
67 pacific; **Supplementary Figure S1**), Walvis Ridge (south Atlantic) and Cicogna (Tethys), an
68 excellent correlation of bulk carbonate $\delta^{13}C$ values has been documented (e.g. Agnini et al., 2015).
69 However, the average value of bulk carbonate $\delta^{13}C$, as well as the magnitude of carbon isotope
70 excursions (CIEs) at any given early Paleogene hyperthermal, e.g. the PETM ca. 56 Ma, varies from
71 one site to another. Major changes in global carbon cycling related to both long- and short-term
72 inputs of CO_2 (Dickens 1995; Dickens et al., 1997; Zachos et al., 2007; 2010) provide a first-order
73 explanation for the correlated changes in bulk carbonate $\delta^{13}C$ records, but the variability between
74 different sites and ocean basins requires a subtler examination of ocean circulation, biogeography,
75 environmental conditions, and diagenesis (Berger and Killingly, 1977; Reuning et al., 2005;
76 Tagliabue and Bopp, 2008, Agnini et al, 2015). In this regard, variations in the $\delta^{13}C$ values and mass
77 fractions of the different components within bulk carbonate may provide additional insight.

78 Here, we compare bulk- and size-fraction-specific isotopic compositions of 45 samples from
79 ODP Site 1209 in Shatsky Rise, north-central Pacific Ocean, accumulated between 58-50 Ma. Our
80 study documents a rise in coarse-fraction (>63 μm) abundance during the PETM, and for several
81 Myr afterwards, at Shatsky Rise. Sites at Walvis Ridge and many other open ocean environments, by
82 contrast, document a decrease in coarse fraction, owing to ocean acidification and thus an increase
83 in carbonate dissolution during the early Paleogene hyperthermals (e.g. Kelly et al., 2010).
84 Therefore, our study indicates that weight percent coarse fraction is not general proxy for carbonate
85 dissolution. Moreover, we also suggest that the increase in coarse fraction at the PETM alters the
86 CIE magnitude at Shatsky Rise compared to other sites.

87

88 **2.1 Site description**

89 Shatsky Rise, a large igneous province in the north-central Pacific, was located at ~15^{o}
90 latitude during early the Paleogene (Bralower et al, 2002; Dutton et al, 2005, **Supplementary**
91 **Figure S1**). Site 1209, drilled during ODP leg 198, lies on the Southern High of Shatsky Rise
92 and contains a continuous Cenozoic record of carbonate sediments. The early Paleogene interval
93 is comprised of clayey nannofossil ooze and nannofossil ooze with clay, along with foraminifers,
94 fish teeth, and biosilica (Bralower et al, 2002). Site 1209 was presumably in the lysoclinal depth
95 range during the early Paleogene, thus constituting a good record of long- and short-term
96 changes in carbonate accumulation and dissolution in the tropical Pacific Ocean (Hancock and
97 Dickens, 2005; Colosimo et al., 2006; Bhattacharya and Dickens, 2020).

98

99 **2.2 Early Paleogene carbon and oxygen isotope records at Shatsky Rise**

100 The basic aspects of carbon and oxygen isotope stratigraphy of the early Paleogene
101 interval at Shatsky Rise have been documented (Luciani et al., 2016; Westerhold et al., 2018;
102 Bhattacharya and Dickens, 2020). Between 58 Ma and 50 Ma, the bulk carbonate $\delta^{13}C$ record
103 consistently tracks that of benthic foraminifers, but with an offset of 1-2‰ (**Figure 2**). Such
104 differences arise because bulk carbonates at Site 1209 are dominated by calcareous nannofossils
105 (Bralower et al., 2002), which are generally finer than 25 μm (Broecker and Clark, 1999; 2009;
106 Reghellin et al, 2015). These nannofossils reflect the higher $\delta^{13}C$ values of inorganic carbon in
107 surface water (**Figure 1**; Reghellin et al., 2020; Bhattacharya and Dickens, 2020). Benthic
108 foraminifers, however, represent bottom-water conditions characterized by lower $\delta^{13}C$ values
109 (**Figure 1**), resulting in consistently lower $\delta^{13}C$ values than bulk carbonates (**Figure 2**). In

contrast, $\delta^{18}O$ values of bulk carbonates between 58 Ma and 54 Ma are lower than that of benthic foraminifers (**Figure 2**), because bottom waters are generally cooler than surface waters (**Figure 1**). Between 54-51 Ma, the difference between bulk carbonate- and benthic foraminiferal $\delta^{18}O$ values becomes negligible; a possible collapse in the temperature gradient in the stratified waters of early Eocene has been implicated (e.g. Kaiho et al., 2006; Hines et al., 2017; Barnet et al., 2020). After 51 Ma, however, benthic foraminiferal $\delta^{18}O$ values become lower than those of bulk carbonates. Here it is important to note that the carbonate sediments from Shatsky Rise show significant diagenetic alterations that may have altered the bulk-carbonate $\delta^{18}O$ isotopic record and thus its apparent relationship to benthic foraminiferal $\delta^{18}O$ values (Dutton et al., 2005; Bhattacharya and Dickens, 2020).

In general, both planktic and benthic foraminifers in open marine sediments (e.g., Site 1209) constitute the bulk of the coarse fraction, which is generally >63 μm (Chiu and Broecker, 2008; Frenz et al., 2005; Bassinot et al, 1994). However, due to diverse ecological niches, the resultant isotopic compositions of the various genera, especially of the planktic foraminifers, vary greatly (**Figure 1; 2**). Spinose planktic foraminifers like *Morozovella sp*. and *Acarinina sp*. have higher $\delta^{13}C$ values than bulk carbonates, while non-spinose planktic foraminifers like *Subbotina sp*., have $\delta^{13}C$ values largely similar to that of the bulk carbonates (**Figure 2**). Such differences in $\delta^{13}C$ value between these two dominant types of planktic foraminifers of the early Paleogene are often attributed to differences in nutrient profile between the surface and thermocline, which leads to a difference in inorganic carbon uptake and the resultant $\delta^{13}C$ value (e.g. Boersma et al., 1987; Coxall et al., 2000; Makarova et al., 2017). In addition, so-called "vital effects" on isotopic fractionation and photosymbiotic algal associations of mixed surface planktic foraminifers contribute to their higher $\delta^{13}C$ values (e.g. Spero et al., 1991; D'Hondt et

al., 1994; Luciani et al., 2017; Penman et al., 2014; Gaskell and Hull, 2019). The difference in $\delta^{18}O$ values arises primarily from the vertical temperature gradient in the water column. Thus, isotopic differences between planktic foraminifers are thought to reflect growth habitats (**Figure 1**). Therefore, varying proportions of these planktic calcifiers through time may have important implications on the resultant bulk carbonate stable isotope records at any given location.

3. Methods

3.1. Samples and ages

A total of 45 samples (**Supplementary Table 1**) were collected from cores recovered at Site 1209 using a 10 cm^3 wedge. 42 samples are from hole 1209A and 3 samples are from hole 1209C. For this study we use a revised meter composite depth (rmcd) scale (Westerhold and Röhl, 2006). The samples belong to lithostratigraphic subunit IIA of Site 1209, ODP Leg 198 (Bralower et al., 2002) and range between 194.26 and 220.09 rmcd, with ages determined by a previously published astronomically tuned age model (Westerhold et al., 2018).

3.2 Sample processing

All sediment samples were oven-dried at 60˚C for 24 hours to remove residual pore water. Weight measurements before and after drying were recorded. Each dried sample was then split into two portions. One portion weighing ~3g was crushed and homogenized using an agate mortar and used for bulk sediment analyses. The other, weighing ~5g, was used for size-fraction-specific isotope analyses.

Dried samples for size-fraction studies were gently and thoroughly washed in deionized water. The wet sediments were then separated using a stack of 4 sieves: 250 µm, 125 µm, 63 µm

and 25 μm from top to bottom. Each of the five size fractions was then collected on filter paper and left to dry for 24-48 hours at room temperature, after which it was weighed. On an average there was 5.2 ± 4.2 % sample loss associated with the rinsing techniques, details of which can be found in the supplementary information.

Each size fraction was separated into two halves, one of which was crushed and homogenized with agate mortar and used for isotope analyses. The other part was used in stereoscopic and scanning electron microscope (SEM) imagery. Representative samples are shown in **Supplementary Figures S3** and **S4**.

3.3 Stable isotope analyses

Crushed and homogenized bulk sediment samples and size-fraction separates were analyzed for $\delta^{13}C$ and $\delta^{18}O$ values at the Stable Isotope Laboratory at Rice University. Weights of the samples used for these analyses were adjusted to obtain approximately 150 μg of carbonate. They were analyzed on a ThermoScientific Delta V Plus Isotope Ratio Mass Spectrometer (IRMS) coupled with a Gasbench II device. Measurements are reported relative to the Vienna PeeDee Belemnite standard (VPDB) using NBS-18, IAEA-603 and in-house KLS and YALS as standards. The isotopic compositions of these standards are noted in **Table 1**. Analytical precision was 0.05 ‰ and 0.08 ‰ for $\delta^{13}C$ and for $\delta^{18}O$ respectively.

4. Results

4.1 Relative changes in size-fraction abundance

The abundance by weight of each size fraction was normalized to the cumulative weight of all size fractions and is tabulated in **Supplementary Table 2**. In our suite of early Paleogene

sediment samples, fine fraction (FF; <25 μm), is the most abundant size fraction, followed by coarse fraction (CF; >63 μm), and then the intermediate fraction (IF; 25-63 μm). Their abundance by weight, on average, is 91 wt%, 7 wt%, and 2 wt%, respectively (see also **Figures 3, 4** and **Supplementary Figure S5**). Among the three sub-fractions of CF, the 125-250 μm fraction dominates (mean 5 wt%), followed by the 63-125 μm fraction (mean 2 wt%), and then the >250 μm size fraction (mean 0.1 wt%).

The relative abundance of FF decreases notably near the PETM, where it reaches a minimum (from >95% to ~75 wt% at 56 Ma**;** see **Figure 3** and **Supplementary Figure S5**). This decrease in FF abundance coincides with a maximum in CF and IF abundances. These relative proportions persist until ~54 Ma. Between 53- and 51 Ma, the size-fraction abundances return to levels more characteristic of the 58-56 Ma time period.

4.2 Carbon isotopic composition of bulk sediments and size fractions

The $\delta^{13}C$ composition of bulk carbonates and size fractions is tabulated in **Supplementary Table S3.** All size fractions show a $\delta^{13}C$ trend similar to that of bulk carbonate through the 58-50 Ma interval (i.e., that shown in **Figure 2**; see **Supplementary Figure S6**). A prominent negative CIE of ~2.25 ‰ occurs at ~55.9 Ma. Another prominent negative CIE of ~0.9 ‰ occurs at ~54 Ma. Between 56-53 Ma, the $\delta^{13}C$ values of the size fractions and bulk sedimentary carbonates exhibit a decreasing trend up-section. After 52 Ma, there is a ~1‰ increase in $\delta^{13}C$ values of bulk sedimentary carbonates as well as size-fraction separates, followed by a broader $\delta^{13}C$ increase up-section.

The FF $\delta^{13}C$ value is similar to the bulk-carbonate $\delta^{13}C$ value, although the former is generally slightly higher (**Figure 3**). The overall CF $\delta^{13}C$ value is ~0.5 ‰ lower than the bulk-

carbonate $\delta^{13}C$ value before the PETM, but a notable change in the CF $\delta^{13}C$ trend occurs at ~55.9 Ma (**Figure 3**): immediately after the PETM, CF $\delta^{13}C$ values become consistently higher than the bulk-carbonate $\delta^{13}C$ values until ~54 Ma. Then, between 54-51 Ma, this difference tends to decrease up the section. Both the 63-125 μm and 125- 250 μm size fractions follow this trend; however, the $\delta^{13}C$ value of >250 μm size fractions is generally higher than bulk-carbonate $\delta^{13}C$ throughout the early Paleogene interval.

4.3 Oxygen isotope composition of bulk sediments and size fractions

The $\delta^{18}O$ of bulk sediments and size fractions are tabulated in **Supplementary Table 4**. A negative oxygen isotope excursion of ~1 ‰ occurs at ~55.9 Ma for both bulk sediments and size fractions (**Supplementary Figure S6**). Between 54-51 Ma, the $\delta^{18}O$ values show a decrease up the section. However, significant amount of fluctuation occurs in the overall $\delta^{18}O$ data at Site 1209.

The bulk carbonate $\delta^{18}O$ is largely similar to FF $\delta^{18}O$, and is generally lower than CF $\delta^{18}O$ (**Figure 4**). However, the sub-fractions of CF show different relationship with bulk carbonate $\delta^{18}O$. The $\delta^{18}O$ value of the 63-125 μm fraction is less than that of bulk carbonate before the PETM, whereas it is higher at and immediately after the PETM. However, the $\delta^{18}O$ value of the 125-250 μm fraction shows an opposing trend: it is higher than that of bulk carbonate before the PETM, and generally lower immediately afterwards. Bulk carbonate $\delta^{18}O$ values are generally higher than those of the 125-250 μm fraction throughout the section.

5. Discussion

224 **5.1 Coherence of $\delta^{13}C$ and $\delta^{18}O$ values in early Paleogene bulk carbonates and size**
225 **fractions**

226 Isotopic mass balance for any given sample dictates that the bulk carbonate stable isotope
227 composition should be equal to the weighted average of its components:

228 (1)

229 Where, *i* represents the different size fractions: <25 μm, 25-63 μm, 63-125 μm, 125-250 μm
230 and >250 μm. The weighted mean isotopic composition of all size fractions is hereafter referred
231 to as the reconstructed bulk isotopic composition.

232 For the present suite of samples, the average difference between reconstructed and
233 measured bulk $\delta^{13}C$ value is 0.01 ± 0.12 ‰ (1σ) (**Figure 5**). Analytical precision of $\delta^{13}C$
234 measurements is 0.05 ‰, so the reconstruction of bulk carbonate $\delta^{13}C$ value from the five size
235 fractions is analytically indistinguishable from the bulk carbonate. Any minor differences that
236 are present may arise from unaccounted mass loss during rinsing and wet sieve separation (~5%
237 by weight), the presence of clays, and/or some differences in homogenization of samples before
238 analysis. For oxygen, the average difference between reconstructed and measured bulk $\delta^{18}O$
239 value is 0.17 ± 0.25 ‰ (1σ) (**Figure 5**), larger than that for carbon isotopes, yet still analytically
240 indistinguishable from the bulk carbonate samples. We note that $\delta^{18}O$ values can be altered due
241 to isotope exchange during sample rinsing and wet sieve separation processes, perhaps leading to
242 a larger variability in the reconstructed $\delta^{18}O$ value. The quantitative consistency between bulk
243 and size-fraction separates, however, suggests that these effects do not affect the interpretations
244 below.

245

246 **5.2 Complexity of coarse-fraction abundance as a proxy for carbonate dissolution**

247 The abundance of >63μm fraction in pelagic sediments, which constitutes the coarse
248 fraction (CF, same as defined in 4.1) has been commonly used as a proxy for carbonate
249 dissolution in paleoceanography (e.g. Bassinot et al., 1994; Kelly et al., 2010). It generally co-
250 varies with lysoclinal depth changes, which control the preservation of planktic foraminifers in
251 pelagic sediments (Broecker and Clark, 1999; Kelly et al, 2005; Littler et al, 2014). Planktic
252 foraminifers show higher vulnerability to carbonate dissolution than benthic foraminifers (e.g.
253 Nguyen et al., 2009); and because benthic foraminifers form only a minor fraction of pelagic
254 carbonate sediments (e.g. Rothwell, 2016), planktic foraminifers constitute the major portion of
255 coarse (or foraminiferal) fraction. During an ocean acidification event, e.g. the PETM or another
256 early Paleogene hyperthermal, enhanced fragmentation and dissolution of planktic foraminiferal
257 tests results in a decrease in CF (Berger et al. 1982; Chiu and Broecker, 2008). Such a response
258 is observed Walvis Ridge in south Atlantic, where a dark colored sediment layer, with low
259 carbonate content and CF, marks the PETM interval (e.g. Zachos et al., 2005; Stap et al., 2009;
260 Kelly et al., 2010).

261 However, studies from other open marine sites have indicated that the CF abundance to
262 does not consistently respond to carbonate dissolution in this manner. At ODP Site 865 in the
263 equatorial Pacific, it remains unusually high in the upper Paleocene and lower Eocene sediment
264 strata and has been attributed to increased winnowing activity by water currents (Arreguin-
265 Rodriguez et al., 2016). Moreover, our results and previous work (Hancock and Dickens, 2005;
266 Westerhold et al., 2018) show an inverted trend in the CF abundance in the early Paleogene
267 sediments at Shatsky Rise (**Figure 6**). In the late Paleocene, CF remains <5 wt %, and reaches a
268 high of ~25 wt % at PETM, and remains substantially high for the next 2 My (**Figure 6**).

An anomalous increase in the test size of certain Morozovellid group planktic foraminifers in the PETM interval at Shatsky Rise has been noted earlier (Kaiho et al., 2006). Presence of algal photosymbionts in these spinose planktic foraminifers possibly give them an ecological advantage in the nutrient-deficient and thermally stratified ocean waters of the PETM (Kaiho et al., 2006). At Site 1209, the absolute abundance of such muricate groups of planktic foraminifers was also high during the PETM, while that of mixed surface dwelling Subbotinids decreased (Petrizzo et al., 2008). Studies show that different groups of planktic foraminifers have a varied response to carbonate dissolution; muricate taxa like *Morozovella* and *Acarinina* are less vulnerable to fragmentation and subsequent dissolution than *Subbotina* (Petrizzo et al., 2008; Nguyen et al., 2011). This resilience could have resulted in enhanced preservation of these photosymbiont-bearing (and possibly thermocline dwelling) planktic foraminifers, even amidst intense ocean acidification and increased carbonate dissolution. Hence, the increase in CF abundance during and after the PETM at Shatsky Rise may be associated with both an increased competitive advantage for photosymbiont-bearing planktic foraminifers and their enhanced preservation.

The environmental conditions that led to such a response of a particular group of planktic foraminifers during the PETM may have been localized, therefore leading to differences in CF abundance in the PETM interval of various open marine sites. Shatsky Rise and Walvis Ridge, for example, were situated in different latitudes during the early Paleogene (**Supplementary Figure 1**). Shatsky Rise, in the tropics, could have experienced higher oligotrophy than Walvis Ridge in the midlatitudes. Greater environmental stress and nutrient deficiency might have made the photosymbiotic relationship in planktic foraminifers an adaptive pathway (Kaiho et al., 2006), resulting in their proliferation at Shatsky Rise. A greater amount of water column

denitrification related to enhanced suboxia in the north-central Pacific has also been suggested for Shatsky Rise during early Eocene (Kast et al., 2019), consistent with nutrient stress at that site. Thus, CF abundance can respond not only to changes in carbonate dissolution but also changes in plankton community composition.

5.3 Partitioning size-fraction contributions to the bulk $\delta^{13}C$ composition and implications for carbon isotope excursions

5.3.1 Fine fraction

Bulk-carbonate $\delta^{13}C$ values are similar to FF $\delta^{13}C$ values throughout the early Paleogene section at Shatsky Rise (**Figure 3**), primarily because the FF is the primary component of bulk carbonate. This observation is similar to that found in the Neogene sediments from the eastern equatorial Pacific (Reghellin et al., 2020) and Paleogene sediments of the Cicogna section (Agnini et al., 2015). The fine fraction, which comprises calcareous nannofossils, tends to record conditions in the upper water column (e.g. Okada and Honjo, 1973; Ennyu et al., 2002), so bulk-carbonate $\delta^{13}C$ values in the early Paleogene interval at Shatsky Rise likely reflect the conditions and $\delta^{13}C$ values of inorganic carbon in surface waters. The IF and CF $\delta^{13}C$ values tend to be markedly different from the bulk $\delta^{13}C$ value. These size fractions contain both planktic and benthic foraminifers, the so their $\delta^{13}C$ values reflect a mixed signal of surface- and bottom-water carbon-isotope composition (**Figure 1**).

5.3.2 Intermediate fraction

Because most calcareous nannofossils are <25 μm in test size, and foraminifers are generally >63 μm, the IF is likely comprised of juvenile and fragmented adult foraminifers.

315 However, because IF is a mix of both planktic and benthic foraminifers, interpreting its $\delta^{13}C$
316 value is less straightforward.

317 The bulk carbonate $\delta^{13}C$ is generally higher than IF $\delta^{13}C$, possibly because of the
318 presence of small sized benthic foraminifers. During early Paleogene hyperthermals, deep-sea
319 benthic foraminifers underwent significant extinction, loss in diversity and reduction in test size
320 (Kaiho et al., 2006; Thomas, 2007; Alegret et al., 2009; Foster et al., 2013), and could constitute
321 a major proportion of the IF, resulting in lower $\delta^{13}C$ values, compared to the bulk carbonate
322 (**Figure 3**).

323 Within the PETM interval, the IF abundance increases (**Figure 3**). The widespread ocean
324 acidification and shoaling of carbonate saturation horizons associated with the PETM could have
325 resulted in increased planktic foraminiferal fragmentation (e.g. Hancock and Dickens, 2005;
326 Colossimo et al., 2006; Bhattacharya and Dickens, 2020), and the breakage of larger
327 foraminiferal tests could increase IF abundance at the PETM interval. In our data, the difference
328 between IF and bulk-carbonate $\delta^{13}C$ values shrinks at the PETM (**Figure 3**), consistent with a
329 larger contribution from ^{13}C-enriched planktic foraminifer fragments. We note that another
330 increase in IF abundance is evident between 54.5 and 53.5 Ma. Despite a low sampling
331 resolution of this study, this increase in IF is also plausibly explained by enhanced carbonate
332 dissolution and foraminiferal fragmentation around the H1/ETM2 hyperthermal event.
333
334 **5.3.3 Coarse fraction**

335 The change in CF $\delta^{13}C$ value from lower than to higher than the bulk carbonate $\delta^{13}C$
336 value across the PETM at Shatsky Rise (**Figure 7**) is particularly striking. It may result from two
337 key changes to foraminiferal communities that occurred. First, the PETM caused significant

benthic foraminiferal extinction (e.g. Thomas, 2007; Alegret et al., 2009). Benthic foraminifers have lower $\delta^{13}C$ values than the calcareous nannoplanktons and planktic foraminifers (**Figure 1**), so removal of benthic foraminiferal mass increases the bulk $\delta^{13}C$ values toward those of the planktic species. Second, a marked increase in the CF abundance at Shatsky Rise (**Figure 6**) may result from an increase in relative abundance and size, and better preservation of photosymbiont-bearing planktic foraminifers, e.g. *Morozovella* (Kaiho et al., 2006; Petrizzo et al., 2008; Ngyuen et al., 2011), which have the highest $\delta^{13}C$ value among all the components of bulk carbonates (**Figures 1 and 2**). An increase in Morozovellids and Acarinids from 200/g to 2900/g of bulk sediments was reported across the PETM at Site 1209 in Petrizzo et al. (2008). This increase in the proportion of high-$\delta^{13}C$ components in the bulk carbonate system across the PETM interval would increase the resultant bulk-carbonate $\delta^{13}C$ value.

Here we examine the importance of this effect using the mass-balance framework (Eq. 1) for the FF, IF, and CF components. For this quantitative analysis, we further divide CF into three sub-components: benthic foraminifers (B in **Figure 8A**), planktic foraminifers with photosymbionts (e.g. *Morozovella sp.* and *Acarinina sp.*; M/A in **Figure 8A**), and planktic foraminifers without photosymbionts (e.g. *Subbotina sp.*; S in **Figure 8A**). All three sub-components have known $\delta^{13}C$ values before, during, and after the PETM (Dutton et al., 2005; Westerhold et al., 2018). These common early Paleogene varieties of planktic foraminifers have distinct carbon isotope compositions (**Figure 2** and Makarova et al., 2017; Gaskell and Hull, 2019). Thus, we can now define the $\delta^{13}C_{CF}$ mass balance in the same way as in Eq. 1:

(2)

with (wt%) here representing the weight percent within the coarse fraction only. While $(wt\%)_B$, $(wt\%)_{M/A}$, and $(wt\%)_S$ are unknown, the known $\delta^{13}C$ values of the three sub-components are

361 listed in **Table 2**. We determined plausible relative weight percent of the three components that
362 can reproduce the measured $\delta^{13}C_{CF}$ value before, during, and after the PETM. An increase in
363 $(wt\%)_{M/A}$ and decrease in $(wt\%)_{B}$ within the CF system was, indeed, necessary (**Table 2; Figure**
364 **8**): a decline in $(wt\%)_{B}$ without an increase in $(wt\%)_{M/A}$ cannot reproduce the measured $\delta^{13}C_{CF}$
365 value at the PETM. It is important to note here that this simplified representation of the CF mass
366 balance omits several other genera of planktic foraminifers that existed in early Paleogene
367 oceans. Though imprecise, our results broadly corroborate the plausibility of the M/A increase in
368 the PETM scenario presented above for Shatsky Rise and the isotopic data do not rule out such a
369 planktonic community shift. Thus, it also suggests that size fraction abundances can strongly
370 influence bulk sedimentary $\delta^{13}C$ values in the early Paleogene.
371
372 **5.3.4 The magnitude of PETM carbon isotope excursion at Shatsky Rise**
373 Changing community structures of marine calcifiers during the anomalous warmth of the
374 PETM as seen at Shatsky Rise may have further implications on carbon isotope excursions. Here
375 we revisit the bulk $\delta^{13}C$ record of the PETM interval at Shatsky Rise (Dickens and Backman,
376 2013; Luciani et al., 2016; Bhattacharya and Dickens, 2020), Walvis Ridge (Kelly et al., 2010;
377 Westerhold et al., 2017), and Cicogna (Agnini et al., 2015). The bulk $\delta^{13}C$ values of the three
378 sites are offset, as are the magnitudes of the PETM CIEs: the difference between average $\delta^{13}C$
379 values before the CIE (from 56.1-55.93 Ma) and the lowest $\delta^{13}C$ value measured within the CIE
380 interval, are 3.1‰ at Walvis Ridge, 2.75‰ at Cicogna and 2.25‰ at Shatsky Rise (**Figure 6C**).
381 Multiple factors could have contributed to these differences in the bulk $\delta^{13}C$ values. Site
382 depth and location are both important. For example, the Cicogna section was deposited in water
383 depths <1000m, in a mid-lower bathyal setting (Giusberti et al., 2007; 2016), which is proximal

384 to organic matter rich terrigenous sediment source; hence, the $\delta^{13}C$ values of the carbonates there
385 can differ from those in open marine environments. This discrepancy in depositional
386 environment could result in consistently lower $\delta^{13}C$ values in the Cicogna bulk carbonates than
387 at Shatsky Rise and Walvis Ridge. In addition, the latitude and location within an ocean basin
388 can influence $\delta^{13}C$ values of dissolved inorganic carbonate: modern upwelling regions, for
389 example, have lower $\delta^{13}C$ values than in the oligotrophic ocean (e.g. Tagliabue and Bopp, 2008).
390 The interplay of these factors can lead to differences in the makeup of bulk carbonates
391 and thus spatial variations in the bulk carbonate $\delta^{13}C$ values, especially during CIEs. For
392 example, across the PETM onset interval, the CF abundance drops from 4 wt.% to 1 wt.% at
393 Walvis Ridge, but rises from 7 wt.% to 20 wt.% at Shatsky Rise (**Figure 6B**), presumably due to
394 the proliferation of Morozovellids and other photosymbiont-bearing planktic foraminifera. The
395 pronounced increase in these communities during the PETM in the north-central Pacific Ocean
396 (**Figure 8**) may have dampened the magnitude of the Paleocene-Eocene CIE at Shatsky Rise
397 because they exhibit the highest $\delta^{13}C$ values amongst all the components of pelagic carbonates;
398 increasing their abundance in the bulk carbonate system would result in a higher $\delta^{13}C$ value (i.e.,
399 a less negative excursion) within the CIE interval. While the precise evolution of relative
400 community abundances is not well constrained by the isotopic data, a change in the proportion of
401 planktic and benthic foraminifera (by mass) during the PETM is required to explain the
402 magnitude of the CIE at Shatsky Rise (see **Table 2**).
403
404 **5.4 Interpreting size-fraction specific $\delta^{18}O$ variations**
405 Unlike the $\delta^{13}C$ record, size-fraction specific $\delta^{18}O$ variations at Shatsky Rise are
406 complicated by post-depositional effects. In the hothouse (ice-free) climate state of the early

Paleogene (Zachos et al., 2001; Zachos et al., 2008; Westerhold et al., 2020), bulk carbonate $\delta^{18}O$ values are expected to reflect upper ocean temperatures because FF (calcareous nannofossils) constitutes its major component (**Figure 4A**; see also Supplementary information). While FF $\delta^{18}O$ values indeed track those of bulk carbonate, the IF $\delta^{18}O$ value is higher than that of bulk carbonate within the PETM interval. One possible explanation for this difference could be a size reduction of benthic foraminifers at PETM, which increases their abundance in the IF and decreases their abundance in the CF (e.g. Kaiho et al., 2006; Thomas, 2007). However, both the FF and IF $\delta^{18}O$ values show fluctuations up section that are similar in magnitude to the PETM change (**Figure 4**), suggesting that the latter may be spurious.

With increasing numbers of photosymbiont-bearing planktic foraminifers and a decreasing abundance of benthic foraminifers within the CF across the PETM interval at Shatsky Rise (**Figure 8**), the difference between CF and bulk $\delta^{18}O$ values is expected to decrease. However, CF $\delta^{18}O$ values remain higher than those in bulk carbonate (**Figure 4C**). In addition, $\delta^{18}O$ values of the >250 μm fraction are consistently lower than those of bulk carbonate (**Figure 4F**), which is the opposite of what is expected: the coarsest component in the bulk carbonates constitutes large planktic foraminifers like muricate Morozovellids (Kaiho et al., 2006), which are believed to dwell in the thermocline, where cooler temperatures should yield higher $\delta^{18}O$ values, not lower. Consequently, size-fraction specific changes in $\delta^{18}O$ values do not obviously reflect the ecological trends inferred from of $\delta^{13}C$ values; other factors are important.

Dissolution and re-precipitation of carbonates in bulk sediments affects oxygen isotopes greatly in low-latitude open-ocean sites and could increase their $\delta^{18}O$ values (Scholle and Arthur, 1980; Schrag et al., 1995). Indeed, evidence of authigenic calcite and recrystallization of planktic foraminiferal tests have been reported in sediments from Site 1209 (Dutton et al., 2005;

Bhattacharya and Dickens, 2020). The degree of calcite recrystallization varies in different groups of calcifiers, which makes these effects difficult to quantify. Furthermore, calcifiers in the surface oceans (e.g., in the fine fraction) will record a wide range of temperature throughout the year due to seasonal gradients in sea surface temperature, while bottom dwellers will reflect smaller variations in temperature. Consequently, the size-fraction-specific $\delta^{18}O$ values can neither corroborate nor invalidate the interpretations derived from $\delta^{13}C$ values at present.

6. Conclusions

Our study from Shatsky Rise presents variations in bulk carbonate and size fraction $\delta^{13}C$ and $\delta^{18}O$ isotope record and changes in relative abundance of different size fractions in the early Paleogene interval between 58 and 50 Ma. Bulk carbonate $\delta^{13}C$ values have been commonly used in chemostratigraphic correlation of widely separated marine sedimentary sections. Shackleton and Hall (1995) made a pioneering study showing coherency of bulk carbonate $\delta^{13}C$ and $\delta^{18}O$ in the Cenozoic; such records show significant offsets in absolute values through space. While many factors contribute to the spatial variations, our study reveals an additional potential driver of early Paleogene bulk carbonate stable isotope records, namely, variations in the abundances of calcifiers that comprise the bulk carbonates in pelagic depositional environments. The main findings of this study can be hereby summarized:

- Size fraction stable isotope records show comparable temporal trends to those of the bulk carbonates through the early Paleogene interval at Shatsky Rise.
- Consistent with previous studies, bulk $\delta^{13}C$ values primarily track those of surface-dwelling calcareous nannofossils, which yield surface-water signals.

- At Shatsky Rise, an increase in coarse fraction abundance is observed at the PETM, ca. 56 Ma, and persists until ~54 Ma. This increase is associated with an increased abundance of photosymbiont-bearing planktic foraminifers, in contrast to what has been documented in Walvis Ridge in the south Atlantic and in contrast to the simple expectation of increased fragmentation (and therefore a decrease in CF abundance) during ocean acidification events. This observation at Shatsky Rise challenges the generality of CF abundance as a proxy for carbonate dissolution.
- Significant community changes of marine calcifiers during early Paleogene may be a significant driver for resultant heterogeneity in bulk carbonate isotope records across space, even though their temporal trends show good stratigraphic correlation.
- The magnitude of carbon isotope excursions can be modulated by variable abundances of different groups of marine calcifiers at different deep-sea locations. Such effects, along with other factors like latitude and location of site within the ocean basin, can strongly influence the magnitude of a CIE at any given early Paleogene hyperthermal.

Acknowledgement

We thank the scientists and staff at Gulf Coast Repository at College Station for sample collection. This work was partially supported by NSF grant awarded to Cin-Ty Lee, Gerald R. Dickens and colleagues at Rice University and by the 'Program of studying abroad for young scholars' awarded to Lin Cong by Northeast Petroleum University. All data in the manuscript are available in Tables in the main text and as Supplementary Tables in supporting information during review process. All data will be finally deposited into Pangaea database upon acceptance of the manuscript.

References

Agnini, C., Spofforth, D., Dickens, G., Rio, D., Pälike, H., Backman, J., et al. (2016). Stable isotope and calcareous nannofossil assemblage record of the late Paleocene and early Eocene (Cicogna section). Climate of the Past (Vol. 12). https://doi.org/10.5194/cp-12-883-2016

Alegret, L., Ortiz, S., & Molina, E. (2009). Extinction and recovery of benthic foraminifera across the Paleocene-Eocene Thermal Maximum at the Alamedilla section (Southern Spain). Palaeogeography, Palaeoclimatology, Palaeoecology, 279(3–4), 186–200. https://doi.org/10.1016/j.palaeo.2009.05.009

Arreguín-Rodríguez, G. J., Alegret, L., & Thomas, E. (2016). Late Paleocene-middle Eocene benthic foraminifera on a Pacific seamount (Allison Guyot, ODP Site 865): Greenhouse climate and superimposed hyperthermal events. Paleoceanography, 31(3), 346–364. https://doi.org/10.1002/2015PA002837

Barnet, J. S.K., Littler, K., Westerhold, T., Kroon, D., Leng, M. J., Bailey, I., et al. (2019). A High-Fidelity Benthic Stable Isotope Record of Late Cretaceous–Early Eocene Climate Change and Carbon-Cycling. Paleoceanography and Paleoclimatology, 34(4), 672–691. https://doi.org/10.1029/2019PA003556

Barnet, James S.K., Harper, D. T., LeVay, L. J., Edgar, K. M., Henehan, M. J., Babila, T. L., et al. (2020). Coupled evolution of temperature and carbonate chemistry during the Paleocene–Eocene; new trace element records from the low latitude Indian Ocean. Earth and Planetary Science Letters, 545, 116414. https://doi.org/10.1016/j.epsl.2020.116414

Bassinot, F. C., Beaufort, L., Vincent, E., Labeyrie, L. D., Rostek, F., Müller, P. J., et al. (1994).

Coarse fraction fluctuations in pelagic carbonate sediments from the tropical Indian Ocean: A 1500-kyr record of carbonate dissolution. Paleoceanography, 9(4), 579–600. https://doi.org/10.1029/94PA00860

Berger, W., Bonneau, M., & Parker, F. (1982). Foraminifera on the deep-sea floor - lysocline and dissolution rate. Oceanologica Acta, 5(2), 249–258. Retrieved from https://archimer.ifremer.fr/doc/00120/23161/#.XnO_cPaoLlA.mendeley

Berger, W. H., & Killingley, J. S. (1977). Glacial-Holocene transition in deep-sea carbonates: Selective dissolution and the stable isotope signal. Science, 197(4303), 563–566. https://doi.org/10.1126/science.197.4303.563

Bhattacharya, J., & Dickens, G. R. (2020). Eocene carbonate accumulation in the north-central Pacific Ocean: New insights from Ocean Drilling Program Site 1209, Shatsky Rise. Sedimentary Geology, 105705. https://doi.org/10.1016/j.sedgeo.2020.105705

Boersma, A., Silva, I. P., & Shackleton, N. J. (1987). Atlantic Eocene planktonic foraminiferal paleohydrographic indicators and stable isotope paleoceanography. Paleoceanography, 2(3), 287–331. https://doi.org/10.1029/PA002i003p00287

Bralower T.J., I. Premoli Silva, M.J. Malone, et al. Proceedings of the Ocean Drilling Program, Leg, Initial Reports (2002), p. 198, http://www-odp.tamu.edu/publications/198_IR/198ir.htm

Broecker, W., & Clark, E. (2009). Ratio of coccolith $CaCO_3$ to foraminifera $CaCO_3$ in late Holocene deep sea sediments. Paleoceanography, 24(3). https://doi.org/10.1029/2009PA001731

Broecker, W. S., & Clark, E. (1999). $CaCO_3$ size distribution: A paleocarbonate ion proxy? Paleoceanography, 14(5), 596–604. https://doi.org/10.1029/1999PA900016

521 Chiu, T.-C., & Broecker, W. S. (2008). Toward better paleocarbonate ion reconstructions: New
522 insights regarding the $CaCO_3$ size index. Paleoceanography, 23(2), n/a-n/a.
523 https://doi.org/10.1029/2008PA001599
524 Colosimo, A. B., Bralower, T. J., & Zachos, J. C. (2006). EVIDENCE FOR LYSOCLINE
525 SHOALING AT THE PALEOCENE/EOCENE THERMAL MAXIMUM ON SHATSKY
526 RISE, NORTHWEST PACIFIC (Vol. 198). Retrieved from http://www-odp.tamu.edu/
527 Coxall, H. K., Pearson, P. N., Shackleton, N. J., & Hall, M. A. (2000). Hantkeninid depth
528 adaptation: An evolving life strategy in a changing ocean. Geology, 28(1), 87–90.
529 https://doi.org/10.1130/0091-7613(2000)28<87:hdaael>2.0.co;2
530 Cramer, B. S., Toggweiler, J. R., Wright, J. D., Katz, M. E., & Miller, K. G. (2009). Ocean
531 overturning since the late cretaceous: Inferences from a new benthic foraminiferal isotope
532 compilation. Paleoceanography, 24(4). https://doi.org/10.1029/2008PA001683
533 D'Hondt, S., Zachos, J. C., & Schultz, G. (1994). Stable Isotopic Signals and Photosymbiosis in
534 Late Paleocene Planktic Foraminifera. Paleobiology, 20(3), 391–406. Retrieved from
535 https://about.jstor.org/terms
536 D'Onofrio, R., Luciani, V., Dickens, G. R., Wade, B. S., & Kirtland Turner, S. (2020). Demise of
537 the Planktic Foraminifer Genus Morozovella during the Early Eocene Climatic Optimum:
538 New Records from ODP Site 1258 (Demerara Rise, Western Equatorial Atlantic) and Site
539 1263 (Walvis Ridge, South Atlantic). Geosciences, 10(3), 88.
540 https://doi.org/10.3390/geosciences10030088
541 Dickens, G., & Backman, J. (2013). Core alignment and composite depth scale for the lower
542 Paleogene through uppermost Cretaceous interval at Deep Sea Drilling Project Site 577.
543 Newsletters on Stratigraphy (Vol. 46). https://doi.org/10.1127/0078-0421/2013/0027

544 Dickens, G.R. (1995). Dissociation of oceanic methane hydrate as a cause of the carbon isotope
545 excursion at the end of Paleocene. Paleoceanography, 10(6), 965–971.
546 Dickens, Gerald R., Castillo, M. M., & Walker, J. C. G. (1997). A blast of gas in the latest
547 Paleocene: Simulating first-order effects of massive dissociation of oceanic methane
548 hydrate. Geology, 25(3), 259–262. https://doi.org/10.1130/0091-
549 7613(1997)025<0259:abogit>2.3.co;2
550 Dutton, A., Lohmann, K. C., & Leckie, R. M. (2005). Insights from the Paleogene tropical
551 Pacific: Foraminiferal stable isotope and elemental results from Site 1209, Shatsky Rise.
552 https://doi.org/10.1029/2004PA001098
553 Ennyu, A., Arthur, M. A., & Pagani, M. (n.d.). Fine-fraction carbonate stable isotopes as
554 indicators of seasonal shallow mixed-layer paleohydrography. Retrieved from
555 www.elsevier.com/locate/marmicro
556 Foster, L. C., Schmidt, D. N., Thomas, E., Arndt, S., & Ridgwell, A. (2013). Surviving rapid
557 climate change in the deep sea during the Paleogene hyperthermals. Proceedings of the
558 National Academy of Sciences of the United States of America, 110(23), 9273–9276.
559 https://doi.org/10.1073/pnas.1300579110
560 Frenz, M., Baumann, K.-H., Boeckel, B., Hoppner, R., & Henrich, R. (2005). Quantification of
561 Foraminifer and Coccolith Carbonate in South Atlantic Surface Sediments by Means of
562 Carbonate Grain-Size Distributions. Journal of Sedimentary Research, 75(3), 464–475.
563 https://doi.org/10.2110/jsr.2005.036
564 Gaskell, D. E., & Hull, P. M. (2019). Symbiont arrangement and metabolism can explain high
565 δ13c in eocene planktonic foraminifera. Geology, 47(12), 1156–1160.
566 https://doi.org/10.1130/G46304.1

Giusberti, L., Boscolo Galazzo, F., & Thomas, E. (2016). Variability in climate and productivity during the Paleocene–Eocene Thermal Maximum in the western Tethys (Forada section). Climate of the Past, 12(2), 213–240. https://doi.org/10.5194/cp-12-213-2016

Giusberti, Luca, Rio, D., Agnini, C., Backman, J., Fornaciari, E., Tateo, F., & Oddone, M. (2007). Mode and tempo of the Paleocene-Eocene thermal maximum in an expanded section from the Venetian pre-Alps. Bulletin of the Geological Society of America, 119(3–4), 391–412. https://doi.org/10.1130/B25994.1

Hancock, H. J., & Dickens, G. R. (2005). CARBONATE DISSOLUTION EPISODES IN PALEOCENE AND EOCENE SEDIMENT, SHATSKY RISE, WEST-CENTRAL PACIFIC (Vol. 198).

Hines, B. R., Hollis, C. J., Atkins, C. B., Baker, J. A., Morgans, H. E. G., & Strong, P. C. (2017). Reduction of oceanic temperature gradients in the early Eocene Southwest Pacific Ocean. Palaeogeography, Palaeoclimatology, Palaeoecology, 475, 41–54. https://doi.org/10.1016/j.palaeo.2017.02.037

Kaiho, K., Takeda, K., Petrizzo, M. R., & Zachos, J. C. (2006). Anomalous shifts in tropical Pacific planktonic and benthic foraminiferal test size during the Paleocene-Eocene thermal maximum. Paleoceanography, Plaeoclimatology and Paleoecology, 237, 456–464. https://doi.org/10.1016/j.palaeo.2005.12.017

Kast, E. R., Stolper, D. A., Auderset, A., Higgins, J. A., Ren, H., Wang, X. T., et al. (2019). Nitrogen isotope evidence for expanded ocean suboxia in the early Cenozoic. Science, 364(6438), 386–389. https://doi.org/10.1126/science.aau5784

Kelly, D. C., Nielsen, T. M. J., McCarren, H. K., Zachos, J. C., & Röhl, U. (2010). Spatiotemporal patterns of carbonate sedimentation in the South Atlantic: Implications for

carbon cycling during the Paleocene-Eocene thermal maximum. Palaeogeography, Palaeoclimatology, Palaeoecology, 293(1–2), 30–40. https://doi.org/10.1016/j.palaeo.2010.04.027

Littler, K., Röhl, U., Westerhold, T., & Zachos, J. C. (2014). A high-resolution benthic stable-isotope record for the South Atlantic: Implications for orbital-scale changes in Late Paleocene-Early Eocene climate and carbon cycling. Earth and Planetary Science Letters, 401, 18–30. https://doi.org/10.1016/j.epsl.2014.05.054

Luciani, V., Dickens, G. R., Backman, J., Fornaciari, E., Giusberti, L., Agnini, C., & D'Onofrio, R. (2016). Major perturbations in the global carbon cycle and photosymbiont-bearing planktic foraminifera during the early Eocene. Climate of the Past, 12(4), 981–1007. https://doi.org/10.5194/cp-12-981-2016

Luciani, V., D'Onofrio, R., Dickens, G. R., & Wade, B. S. (2017). Did Photosymbiont Bleaching Lead to the Demise of Planktic Foraminifer Morozovella at the Early Eocene Climatic Optimum? Paleoceanography, 32(11), 1115–1136. https://doi.org/10.1002/2017PA003138

Makarova, M., Wright, J. D., Miller, K. G., Babila, T. L., Rosenthal, Y., & Park, J. I. (2017). Hydrographic and ecologic implications of foraminiferal stable isotopic response across the U.S. mid-Atlantic continental shelf during the Paleocene-Eocene Thermal Maximum. Paleoceanography and Paleoclimatology, 32(1), 56–73. https://doi.org/10.1002/2016PA002985

Milliman, J. D. (1993). Production and accumulation of calcium carbonate in the ocean: Budget of a nonsteady state. Global Biogeochemical Cycles, 7(4), 927–957. https://doi.org/10.1029/93GB02524

Nguyen, T. M. P., Petrizzo, M. R., & Speijer, R. P. (2009). Experimental dissolution of a fossil

foraminiferal assemblage (Paleocene-Eocene Thermal Maximum, Dababiya, Egypt): Implications for paleoenvironmental reconstructions. Marine Micropaleontology, 73(3–4), 241–258. https://doi.org/10.1016/j.marmicro.2009.10.005

Nguyen, T. M. P., Petrizzo, M. R., Stassen, P., & Speijer, R. P. (2011). Dissolution susceptibility of Paleocene-Eocene planktic foraminifera: Implications for palaeoceanographic reconstructions. Marine Micropaleontology, 81(1–2), 1–21. https://doi.org/10.1016/j.marmicro.2011.07.001

Okada, H. and Honjo S. (1973). The distribution of oceanic coccolithophorids in the Pacific. Deep-Sea Research, 20

Penman, D. E., Hönisch, B., Zeebe, R. E., Thomas, E., & Zachos, J. C. (2014). Rapid and sustained surface ocean acidification during the Paleocene-Eocene Thermal Maximum. Paleoceanography, 29(5), 357–369. https://doi.org/10.1002/2014PA002621

Petrizzo, M. R., Leoni, G., Speijer, R. P., De Bernardi, B., & Felletti, F. (2008). Dissolution susceptibility of some paleogene planktonic foraminifera from ODP site 1209 (Shatsky rise, Pacific Ocean). Journal of Foraminiferal Research, 38(4), 357–371. https://doi.org/10.2113/gsjfr.38.4.357

Reghellin, D., Coxall, H. K., Dickens, G. R., & Backman, J. (2015). Carbon and oxygen isotopes of bulk carbonate in sediment deposited beneath the eastern equatorial Pacific over the last 8 million years. Paleoceanography, 30(10), 1261–1286. https://doi.org/10.1002/2015PA002825

Reghellin, D., Dickens, G. R., Coxall, H. K., & Backman, J. (2020). Understanding Bulk Sediment Stable Isotope Records in the Eastern Equatorial Pacific, From Seven Million Years Ago to Present Day. Paleoceanography and Paleoclimatology, 35(2).

https://doi.org/10.1029/2019PA003586

Reuning, L., Reijmer, J. J. G., Betzler, C., Swart, P., & Bauch, T. (2005). The use of paleoceanographic proxies in carbonate periplatform settings - Opportunities and pitfalls. Sedimentary Geology, 175(1-4 SPEC. ISS.), 131–152. https://doi.org/10.1016/j.sedgeo.2004.12.026

Rothwell, R. G. (2016). Sedimentary Rocks: Deep Ocean Pelagic Oozes☆. In Reference Module in Earth Systems and Environmental Sciences. Elsevier. https://doi.org/10.1016/b978-0-12-409548-9.10493-2

Sarmiento, J. L., & Gruber, N. (2006). Ocean Biogeochemical Dynamics - Jorge L. Sarmiento, Nicolas Gruber - Google Books. In Ocean biogeochemical dynamics. Retrieved from https://books.google.com/books?hl=en&lr=&id=L16YDwAAQBAJ&oi=fnd&pg=PR1&dq=info:BuV22BEtws0J:scholar.google.com&ots=UU0Fq5VbOx&sig=1p5QoFUrg_ixGNH5P38BukPDSco#v=onepage&q&f=false

Scholle, P. A., & Arthur, M. A. (1980). Carbon isotope fluctuations in Cretaceous pelagic limestones: potential stratigraphic and petroleum exploration tool. American Association of Petroleum Geologists Bulletin, 64(1), 67–87. https://doi.org/10.1306/2f91892d-16ce-11d7-8645000102c1865d

Schrag, D. P., Depaolo, D. J., & Richter, F. M. (1995). Reconstructing past sea surface temperatures: Correcting for diagenesis of bulk marine carbonate. Geochimica et Cosmochimica Acta (Vol. 9).

Shackleton, N. J. (1986). Paleogene stable isotope events. Palaeogeography, Palaeoclimatology, Palaeoecology, 57(1), 91–102. https://doi.org/10.1016/0031-0182(86)90008-8

Shackleton, N.J., Hall, M.A., Bleil, U., Heath, R.G., Buckle, L.H. et al.Carbon isotope

659 stratigraphy Site 577, Initial Rep. Deep Sea Drill. Proj., 86 (1985), pp. 503-512
660 Shackleton, N. J., & Hall, M. A. (1995). Stable isotopes records in bulk sediments (Leg 138),
661 in Proceedings of the Ocean Drilling Program, Scientific Results, vol. 138, edited by Pisias,
662 N. G., L. A. Mayer, T. R. Janecek, A. Palmer Julson, and T. H. van Andel. College
663 Station, 797-805.
664 Slotnick, B. S., Lauretano, V., Backman, J., Dickens, G. R., Sluijs, A., & Lourens, L. (2015).
665 Early Paleogene variations in the calcite compensation depth: new constraints using old
666 borehole sediments from across Ninetyeast Ridge, central Indian Ocean. Climate of the
667 Past, 11(3), 473–493. https://doi.org/10.5194/cp-11-473-2015
668 Slotnick, Benjamin S, Dickens, G. R., Nicolo, M. J., Hollis, C. J., Crampton, J. S., Zachos, J. C.,
669 & Sluijs, A. (2012). Large-Amplitude Variations in Carbon Cycling and Terrestrial
670 Weathering during the Latest Paleocene and Earliest Eocene: The Record at Mead Stream,
671 New Zealand. The Journal of Geology, 120(5), 487–505. https://doi.org/10.1086/666743
672 Spero, H. J., Lerche, I., & Williams, D. F. (1991). Opening the carbon isotope “vital effect” black
673 box, 2, Quantitative model for interpreting foraminiferal carbon isotope data.
674 Paleoceanography, 6(6), 639–655. https://doi.org/10.1029/91PA02022
675 Stap, L., Sluijs, A., Thomas, E., & Lourens, L. (2009). Patterns and magnitude of deep sea
676 carbonate dissolution during Eocene Thermal Maximum 2 and H2, Walvis Ridge,
677 southeastern Atlantic Ocean. Paleoceanography,
678 24(1).https://doi.org/10.1029/2008PA001655
679 Tagliabue, A., & Bopp, L. (2008). Towards understanding global variability in ocean carbon-13.
680 Global Biogeochemical Cycles, 22(1). https://doi.org/10.1029/2007GB003037
681 Thomas, E. (2007). Cenozoic mass extinctions in the deep sea: What perturbs the largest habitat

682 on Earth, in: Large Ecosystem Perturbations: Causes and Consequences, edited by:
683 Monechi, S., Coccioni, R., and Rampino, M., Geol. S. Am. S., Boulder, Colorado, The
684 Geological Society of America, 424, 1–23.
685 Westerhold, T., Röhl, U., Donner, B., & Zachos, J. C. (2018). Global Extent of Early Eocene
686 Hyperthermal Events: A New Pacific Benthic Foraminiferal Isotope Record From Shatsky
687 Rise (ODP Site 1209). Paleoceanography and Paleoclimatology, 33(6), 626–642.
688 https://doi.org/10.1029/2017PA003306
689 Westerhold, Thomas, & Röhl, U. (2006). REVISED COMPOSITE DEPTH RECORDS FOR
690 SHATSKY RISE SITES 1209, 1210, AND 1211 (Vol. 198). Retrieved from http://www-
691 odp.tamu.edu/
692 Westerhold, Thomas, Röhl, U., Frederichs, T., Agnini, C., Raffi, I., Zachos, J. C., & Wilkens, R.
693 H. (2017). Astronomical calibration of the Ypresian timescale: implications for seafloor
694 spreading rates and the chaotic behavior of the solar system? Climate of the Past, 13(9),
695 1129–1152. https://doi.org/10.5194/cp-13-1129-2017
696 Westerhold, Thomas, Marwan, N., Drury, A. J., Liebrand, D., Agnini, C., Anagnostou, E., et al.
697 (2020). An astronomically dated record of Earth's climate and its predictability over the last
698 66 million years. Science, 369(6509), 1383–1387. https://doi.org/10.1126/science.aba6853
699 Zachos, J., Pagani, M., Sloan, L., Thomas, E., & Billups, K. (2001). Trends, Rhythms, and
700 Aberrations in Global Climate 65 Ma to Present. Science, 292(5517), 686–693.
701 https://doi.org/10.1126/science.1059412
702 Zachos, J. C., Röhl, U., Schellenberg, S. A., Sluijs, A., Hodell, D. A., Kelly, D. C., et al. (2005).
703 Paleoclimate: Rapid acidification of the ocean during the paleocene-eocene thermal
704 maximum. Science, 308(5728), 1611–1615. https://doi.org/10.1126/science.1109004

Zachos, J. C., Bohaty, S. M., John, C. M., McCarren, H., Kelly, D. C., & Nielsen, T. (2007). The Palaeocene-Eocene carbon isotope excursion: Constraints from individual shell planktonic foraminifer records. Philosophical Transactions of the Royal Society A: Mathematical, Physical and Engineering Sciences, 365(1856), 1829–1842. https://doi.org/10.1098/rsta.2007.2045

Zachos, J. C., Dickens, G. R., & Zeebe, R. E. (2008, January 17). An early Cenozoic perspective on greenhouse warming and carbon-cycle dynamics. Nature. Nature Publishing Group. https://doi.org/10.1038/nature06588

Zachos, J. C., McCarren, H., Murphy, B., Röhl, U., & Westerhold, T. (2010). Tempo and scale of late Paleocene and early Eocene carbon isotope cycles: Implications for the origin of hyperthermals. Earth and Planetary Science Letters, 299(1–2), 242–249. https://doi.org/10.1016/j.epsl.2010.09.004

718 **Tables and table captions**

719

720 **Table 1**: Carbon and oxygen isotopic composition of standard reference materials used.

721

Standard material name	NBS-18	IAEA-603	In House-KLS	In House-YALS
Material description	calcite	calcite	limestone	limestone
$\delta^{13}C$‰ (VPDB)	-5.01	2.46	0.33	1.15
$\delta^{18}O$‰ (VPDB)	-22.97	-2.37	-29.98	-6.08

722

723 **Table 2**: Values of the known and unknown variables in Eqn 2. The $\delta^{13}C$ of CF (measured), B,
724 M/A, and S are known variables. The wt% of B, M/A, and S are generated by optimization of
725 modeled $\delta^{13}C_{CF}$.
726
727
728
729
730
731
732
733
734
735

	pre-PETM	at-PETM	post-PETM
$\delta^{13}C_B$ / ‰	0.5	-0.75	0.75
$\delta^{13}C_{M/A}$ / ‰	3.20	1.25	2.50
$\delta^{13}C_S$ / ‰	2.25	0.50	1.75
Modeled $(wt\%)_B$	45	20	20
Modeled $(wt\%)_{M/A}$	47	78	73
Modeled $(wt\%)_S$	8	2	7
$\delta^{13}C_{CF}$ / ‰ (modeled)	1.91	0.84	2.10
$\delta^{13}C_{CF}$ / ‰ (measured)	1.93	0.72	2.14

Figures and figure captions

Figure 1

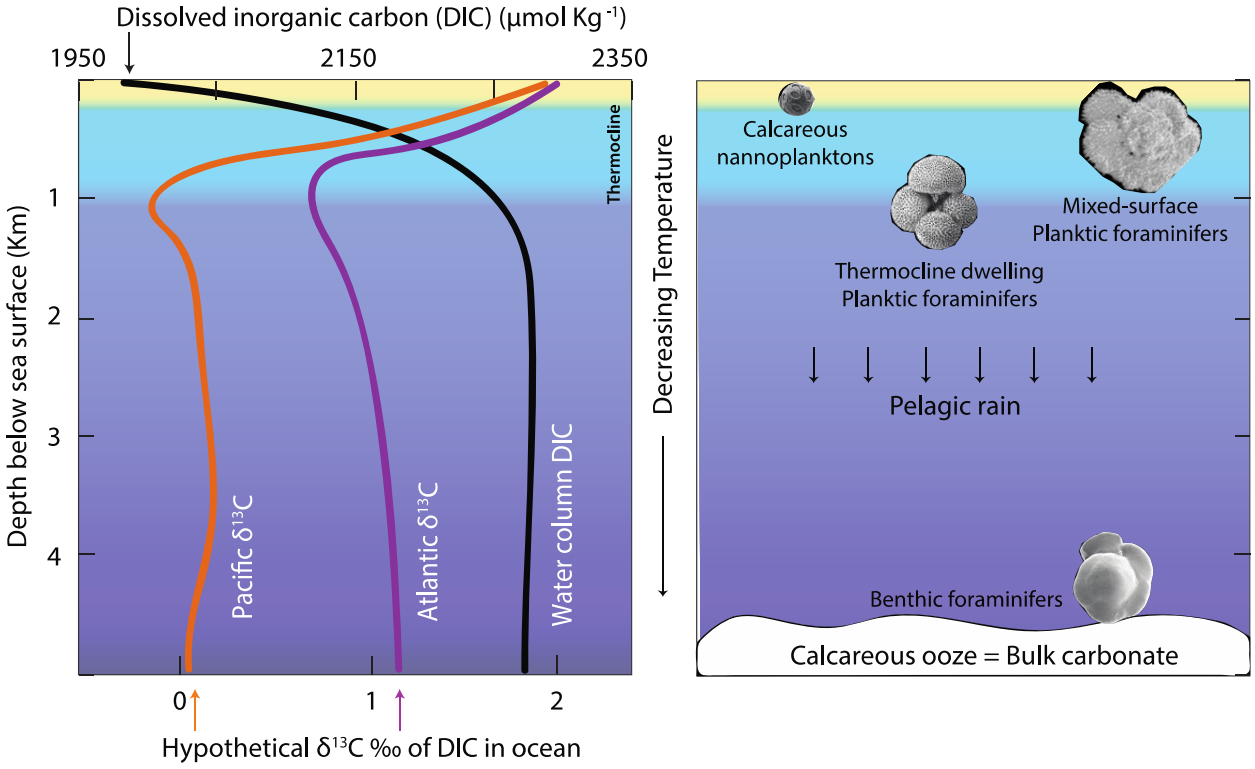

Constituents of bulk carbonate in deep marine carbonate records and their variable $\delta^{13}C$ compositions. Pelagic components (primarily originating from mixed surface waters and thermocline) constitute calcareous nannofossils and planktic foraminifers. Benthic foraminifers, constituting the benthic factory, are bottom dwellers. The orange and purple lines show variations in modern day DIC $\delta^{13}C$ in the Pacific and Atlantic oceans respectively. The black line shows change in temperature with depth in ocean water column.

748 **Figure 2**

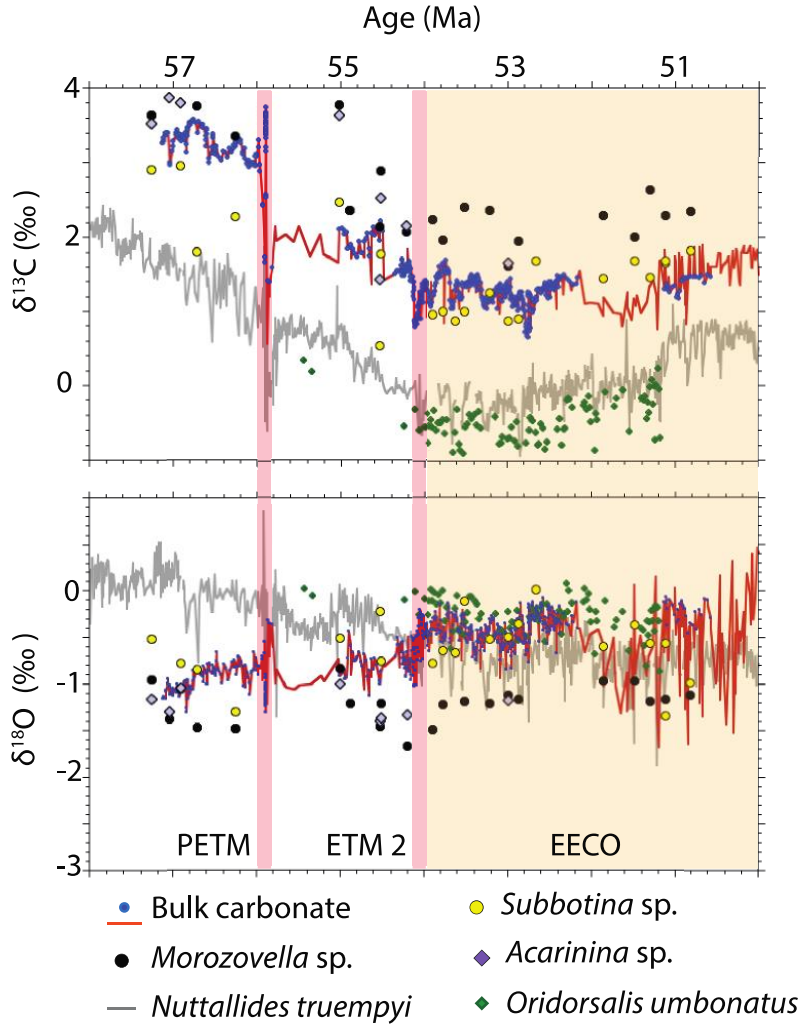

749

750

751 **Previously published early Eocene carbon and oxygen stable isotope records from Shatsky**
752 **Rise.** Early Paleogene bulk (Dickens and Backman, 2013; Luciani et al., 2016; Bhattacharya and
753 Dickens, 2020), benthic (Westerhold et al., 2018) and planktic foraminiferal (Dutton et al., 2005
754 and Shackleton et al., 1985) stable carbon and oxygen isotope record at Shatsky Rise.

Figure 3

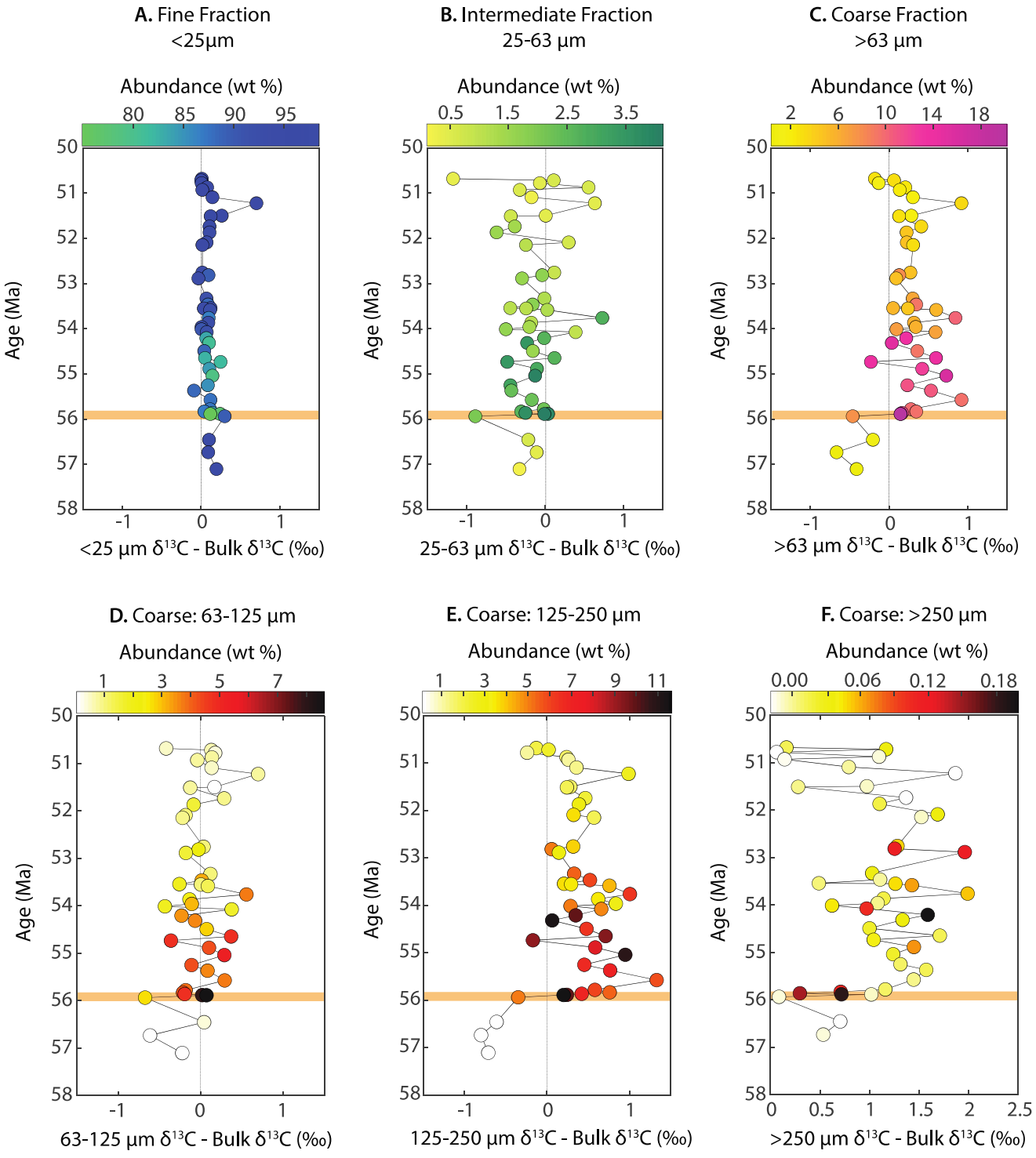
A. Fine Fraction
<25µm
Abundance (wt %)
80 85 90 95
B. Intermediate Fraction
25-63 µm
Abundance (wt %)
0.5 1.5 2.5 3.5
C. Coarse Fraction
>63 µm
Abundance (wt %)
2 6 10 14 18
D. Coarse: 63-125 µm
Abundance (wt %)
1 3 5 7
E. Coarse: 125-250 µm
Abundance (wt %)
1 3 5 7 9 11
F. Coarse: >250 µm
Abundance (wt %)
0.00 0.06 0.12 0.18
Age (Ma)
50 51 52 53 54 55 56 57 58
-1 0 1
0 0.5 1 1.5 2 2.5
<25 µm δ13C - Bulk δ13C (‰)
25-63 µm δ13C - Bulk δ13C (‰)
>63 µm δ13C - Bulk δ13C (‰)
63-125 µm δ13C - Bulk δ13C (‰)
125-250 µm δ13C - Bulk δ13C (‰)
>250 µm δ13C - Bulk δ13C (‰)

Variations in size fraction abundance and their $\delta^{13}C$ values with respect to bulk carbonate $\delta^{13}C$ values across the early Paleogene interval at Shatsky Rise. Changes in abundance (wt %) are color coded for each of the size fractions. The difference between size fraction-specific $\delta^{13}C$ value and bulk carbonate $\delta^{13}C$ value at each sample interval is plotted over time. (A) i-iii show the data for fine fraction FF (<25 μm), IF intermediate fraction (25-63 μm) and coarse fraction CF (>63 μm). (B) in iv-vi, CF is subdivided into three size fractions: 63-125 μm, 125-250 μm and >250 μm. The yellow line denotes PETM interval. The black line provides a visual reference for no difference between size fraction-specific and bulk carbonate $\delta^{13}C$ value.

768 **Figure 4**

769

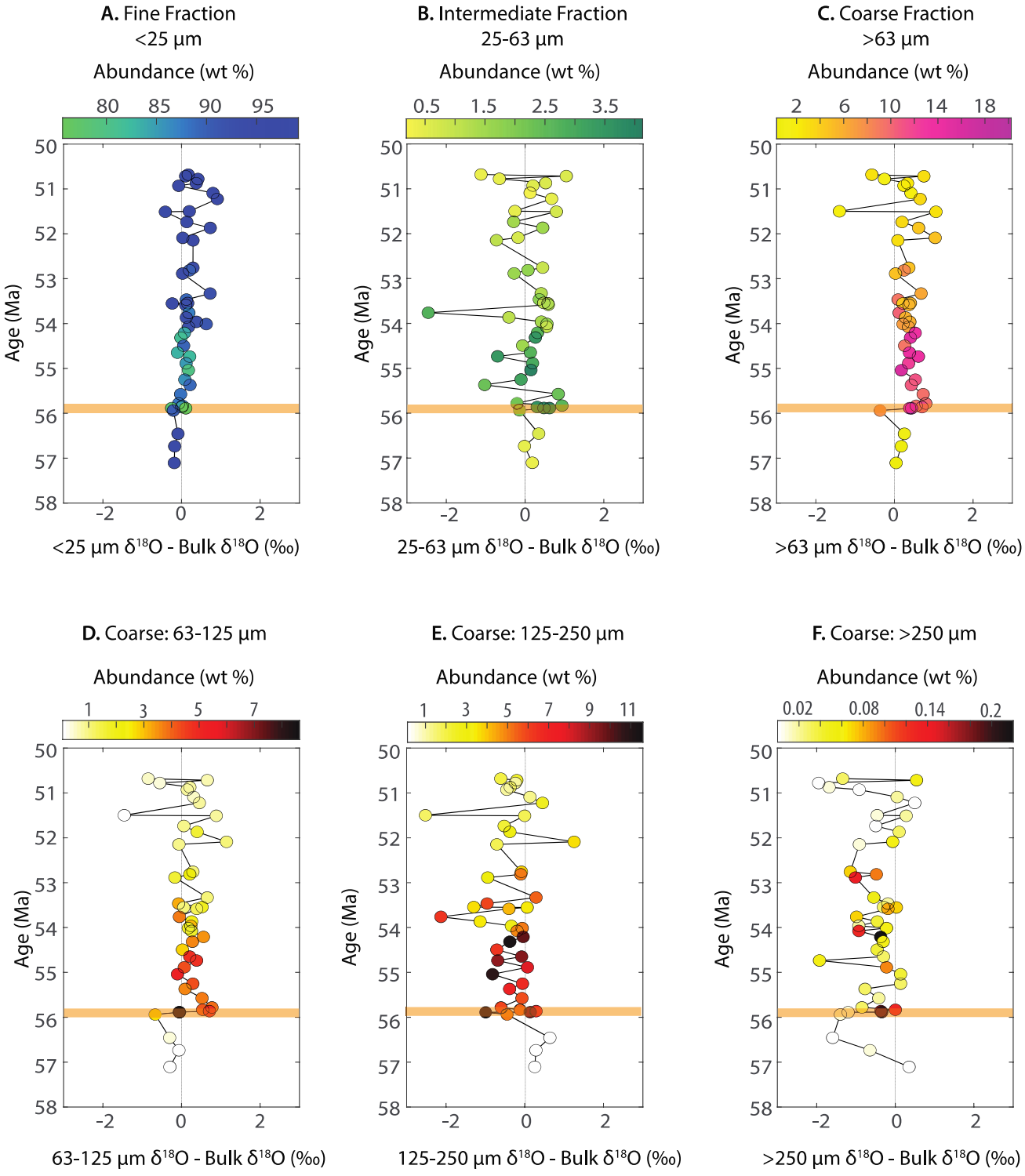

770
771

Variations in size fraction abundance and their $\delta^{18}O$ values with respect to bulk carbonate $\delta^{18}O$ values across the early Paleogene interval at Shatsky Rise. Changes in abundance (wt %) are color coded for each of the size fractions. The difference between size fraction $\delta^{18}O$ and bulk $\delta^{18}O$ at each sample interval is plotted across time. (A) i-iii show the data for fine fraction FF (<25 μm), IF intermediate fraction (25-63 μm) and coarse fraction CF (>63 μm). (B) in iv-vi, CF is subdivided into three size fractions: 63-125 μm, 125-250 μm and >250 μm. The yellow line denotes PETM interval. The black line provides a visual reference for no difference between size fraction-specific and bulk carbonate $\delta^{18}O$ value.

781 **Figure 5**

782

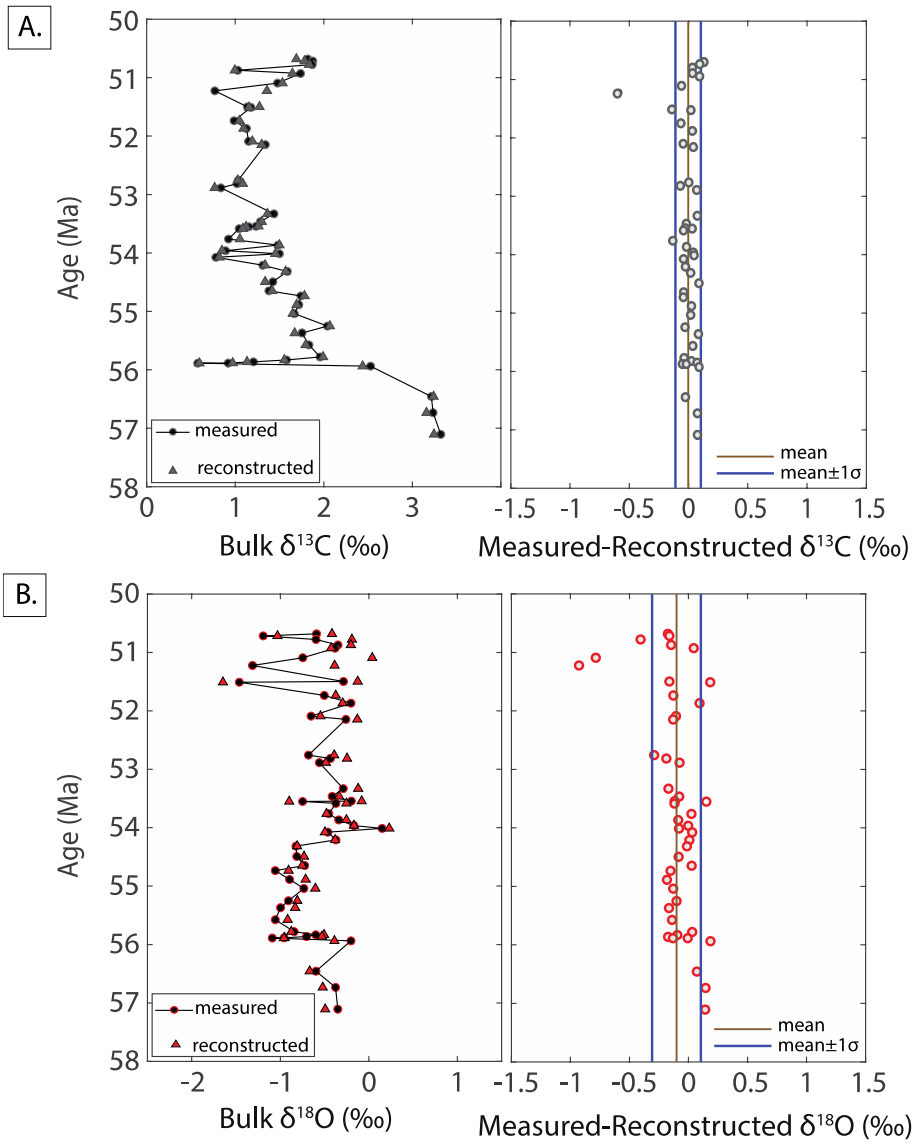

783

784

785 **Difference between measured and size-fraction reconstructed bulk carbon and oxygen**
786 **isotopes.** Left panel shows measured bulk isotope record from Shatsky Rise (solid circles; $\delta^{13}C$
787 in A and $\delta^{18}O$ in B) and the reconstructed bulk isotope values from weighted sums of size
788 fractions (solid rhombs). The right panel shows the difference between measured and
789 reconstructed bulk isotope values.

790 **Figure 6**

791

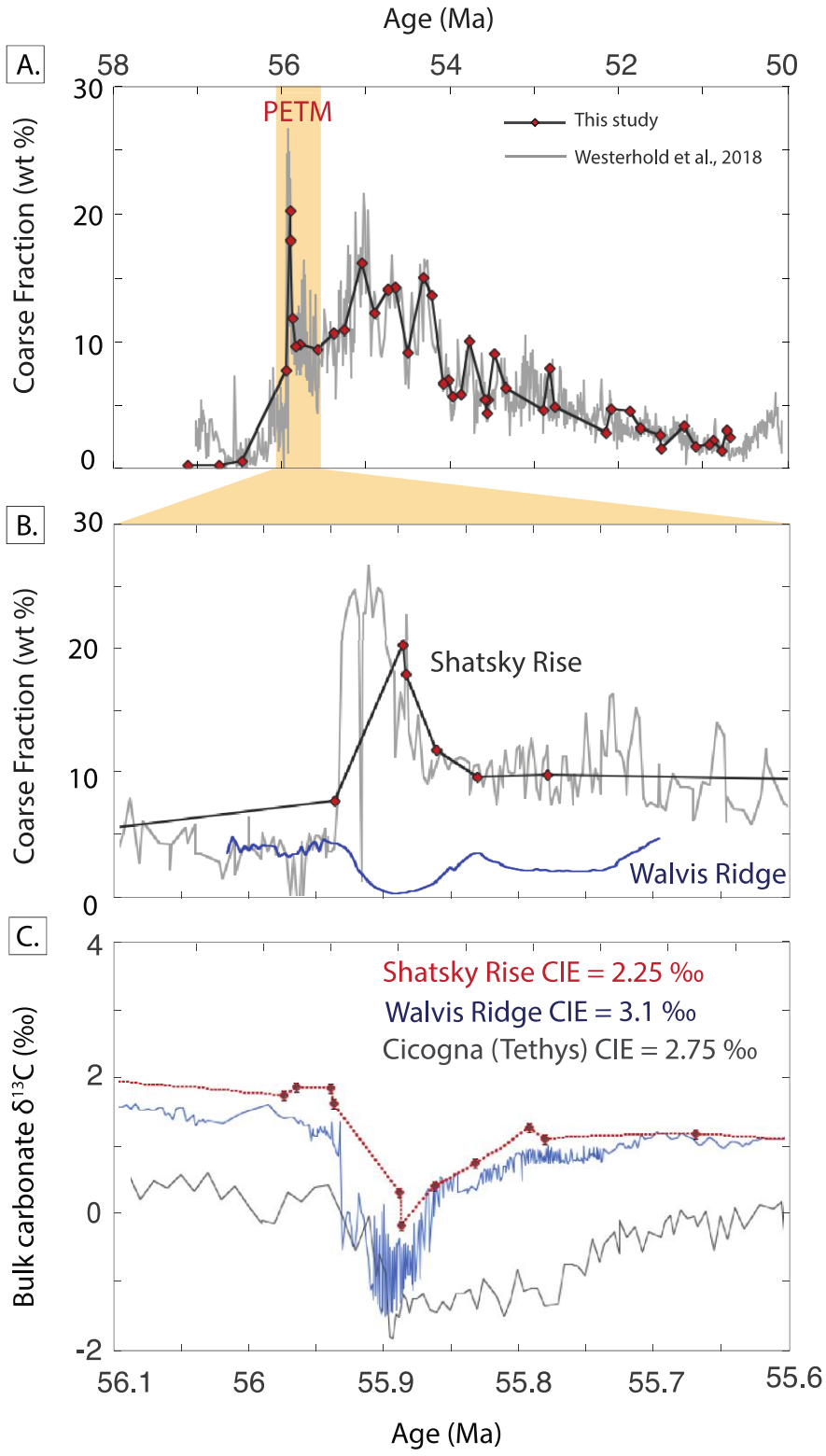

792

Coarse fraction abundance and the PETM CIE at Shatsky Rise and elsewhere. (A) Change in weight percent coarse fraction (WPCF) at Site 1209 between 58-50 Ma. The data from this study is represented by black line with red rhombs, while the grey line in the background constitutes data from Westerhold et al. (2018). (B) Comparison of WPCF at Shatsky Rise and Walvis Ridge across the PETM interval. (C) Comparison of the PETM CIE magnitude for three different open ocean sites: Shatsky Rise (red dashed line), Walvis Ridge (blue line) and Cicogna section in Italy (grey line).

800 **Figure 7**

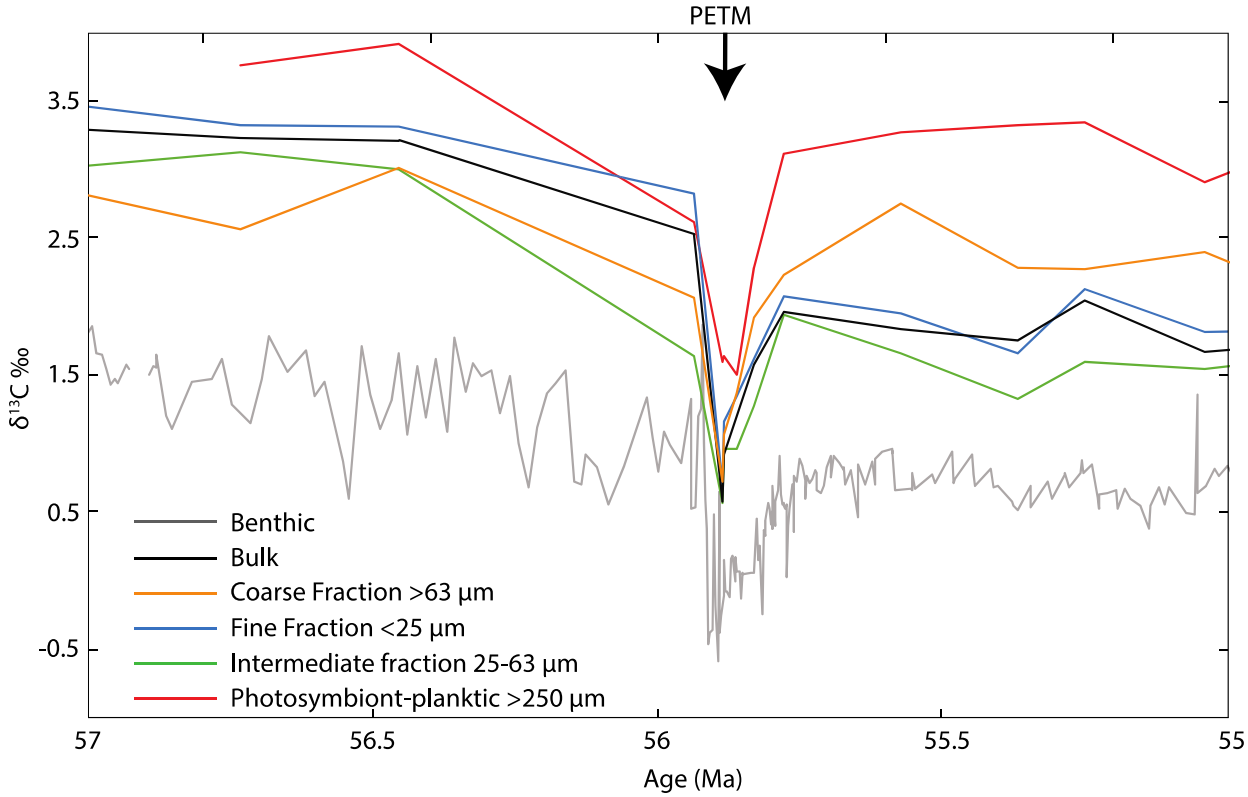

801

802

803 **The $\delta^{13}C$ record of bulk carbonate at Shatsky Rise from 57 – 55 Ma compared to those of**
804 **individual constituents**: benthic foraminifera, fine fraction (calcareous nannofossils),
805 intermediate fraction (fragments and juvenile foraminifers), coarse fraction (mixture of planktic
806 and benthic foraminifers), and larger photosymbiont-bearing planktic foraminifers (>250 µm).

807 **Figure 8**

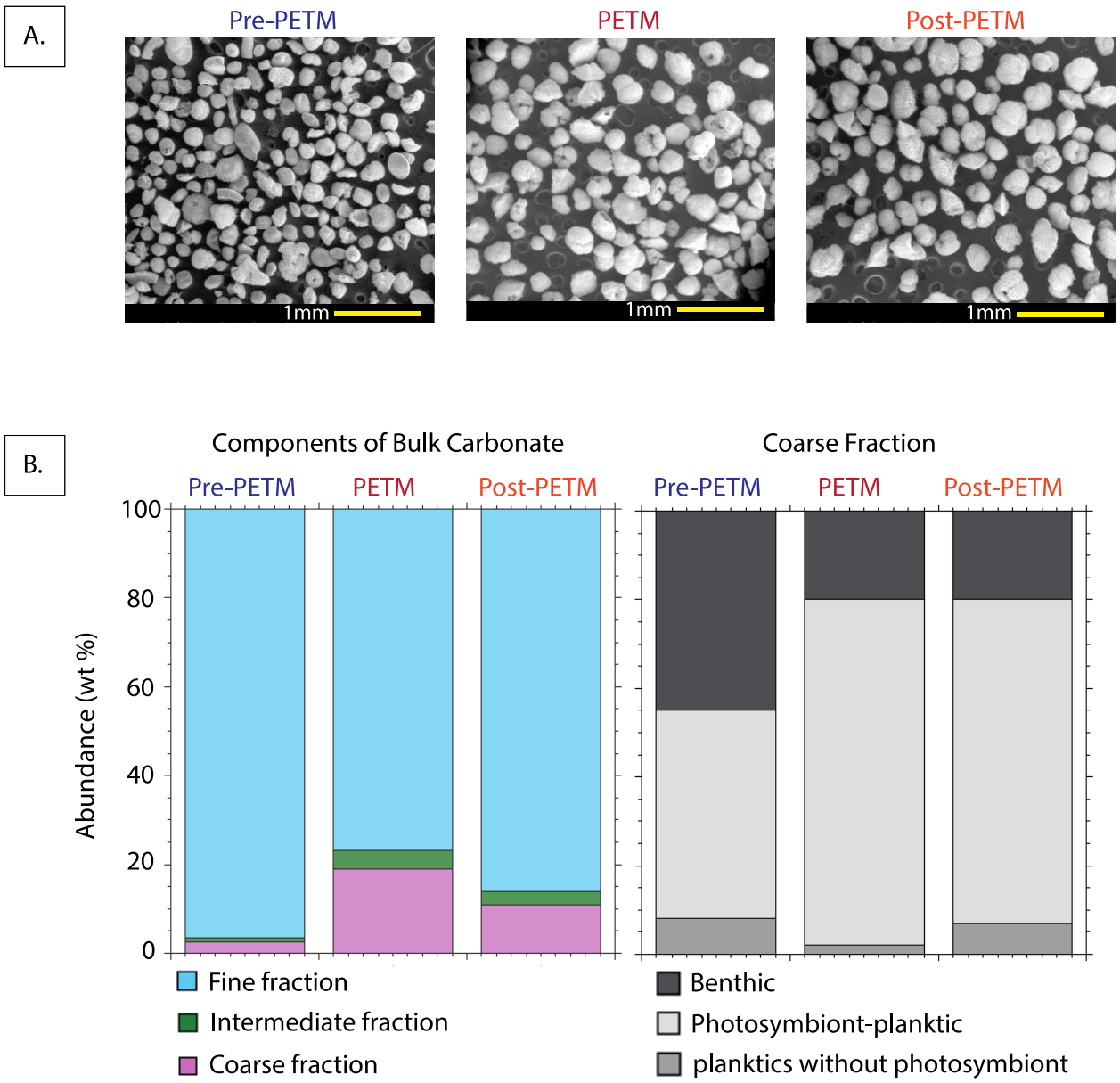

808

809

810

811 **Influence of relative changes in size fraction abundances on the bulk carbonate δ13C**
812 **record at Shatsky Rise.** (A) Three samples from before, during, and after the PETM CIE
813 interval at Site 1209, as seen under SEM. Benthic foraminiferal abundance decreases sharply at

814 and after the PETM, while larger planktic foraminifers increase in abundance. (B) Abundance of
815 benthic foraminifers, photosymbiont-bearing planktic foraminifers, and photosymbiont-free
816 planktic foraminifers for pre-PETM, at-PETM and post-PETM intervals that can quantitatively
817 explain the measured positive shift in CF δ13C value (see 5.3.3).